Theoretical and experimental study of stochastic effects on polarization rotation in a vectorial bistable laser

Kamal P. Singh, Guy Ropars, Marc Brunel, and Albert Le Floch
Laboratoire d'Electronique Quantique—Physique des Lasers, Unité Mixte de Recherche du Centre National de la Recherche Scientifique 6627, Université de Rennes I, Campus de Beaulieu, F-35042 Rennes Cedex, France
(Received 16 February 2005; published 7 March 2006)

We investigate the two-dimensional optical rotor of a weakly modulated vectorial bistable laser submitted to a single or multiple stochastic perturbations. In the Langevin-type equation of the rotor the role of an even or odd input forcing function on the system dynamics is isolated. Through these two inputs of optical and magnetic natures we verify that the stochastic resonance exists only when the periodic modulation acts on the even parity optical input. When two mutually correlated noises are simultaneously submitted to the input functions of opposite parities, we find a critical regime of the noise interplay whereby one stable state becomes noise-free. In this case, the residence time of the light vector in the noise-free state diverges which leads to a collapse of the output signal-to-noise ratio. But, in this critical regime also obtained when one noise drives both the even and odd functions, if the system symmetry is broken through an independent lever control, we can recover the switching cycle due to a new response mechanism, namely, the dual stochastic response, with a specific output signal-to-noise ratio expression. Both the theoretical analysis and the experiment show that the signal-to-noise ratio now displays a robust behavior for a large range of the input noise amplitude, and a plateau with respect to the input signal amplitude. Furthermore, we isolate an original signature of this synchronization mechanism in the residence-time distribution leading to a broadband forcing frequency range. These noise interplay effects in a double well potential are of generic nature and could be found in other nonlinear systems.

DOI: 10.1103/PhysRevA.73.033807 PACS number(s): 42.60.Mi, 42.65.Pc, 02.50.Ey

I. INTRODUCTION

Nonlinear stochastic effects are of wide interest mainly due to the constructive role of noise in the signal detection and information transfer [1]. In this field the most studied phenomenon is stochastic resonance (SR) by which a weak signal can be optimally detected due to the presence of an optimal level of noise [2,3]. But in order to get a significant enhancement of the response in the case of a bistable system through SR some stringent conditions must be satisfied. For instance, the signal amplitude is limited to values close to the system threshold, the noise amplitude must be adjusted around the optimum value, and the frequency detection bandwidth is narrow due to the matching between deterministic and stochastic time scales [2]. Many theoretical attempts were made to improve the stochastic resonance for instance by using arrays of threshold systems [4,5], by employing an extra control signal [6], by using time-modulated correlated noises [7], or through symmetry breaking effects in bistable systems [8,9]. Here we investigate a vectorial optical system, i.e., an optical rotor which can be subjected to perturbations of quite different origins such as of optical, magnetic, or electrical natures. One may wonder how can we identify, in particular experimentally, the symmetry properties of the system perturbed through its various inputs, and what are their roles in the SR based weak signal detection. Moreover, could two noises of different natures interact mutually in such a multi-input system and lead to possible new regimes?

The aim of this paper is to give a detailed theoretical and experimental study of stochastic effects on the polarization rotation in a two-dimensional vectorial bistable laser. With respect to our previous results [10,11], here we focus on providing a further insight in the SR mechanism based on the symmetry properties of the possible modulations and noises. Moreover, we try to derive analytical expressions for the signal-to-noise ratio (SNR) when the optical rotor is subjected to mutually correlated noises and explore the experimental residence-time distributions. We also try to provide a physical picture of the noise interplay in a generic double-well potential.

The paper is organized as follows. In Sec. II we introduce a Langevin-type equation to describe the polarization rotational dynamics in the quasi-isotropic vectorial laser. We emphasize the possibilities due to the multiple inputs of the laser and isolate their symmetry properties. We then derive analytical expressions for the mean residence times and the signal-to-noise ratio when Langevin terms of different natures are mutually correlated. Furthermore, we isolate a so-called dual stochastic response of the laser and highlight its original properties. The predictions coming out of the model are then tested in Sec. III on a laser submitted to various kinds of signals and noises through its optical and magnetic inputs. The experiments are compared to both the analytical expressions and numerical simulations. Finally, Sec. IV provides a summary of results with our conclusions.

II. THEORETICAL ANALYSIS

A. The nonlinear optical rotor model

Let us consider the vectorial bistable laser depicted in Fig. 1(a) oscillating on a single longitudinal mode. The laser cavity is closed by two mirrors M_1 and M_2, and a feeble linear phase anisotropy $\Delta\Phi_{xy}$ is introduced inside the cavity. The

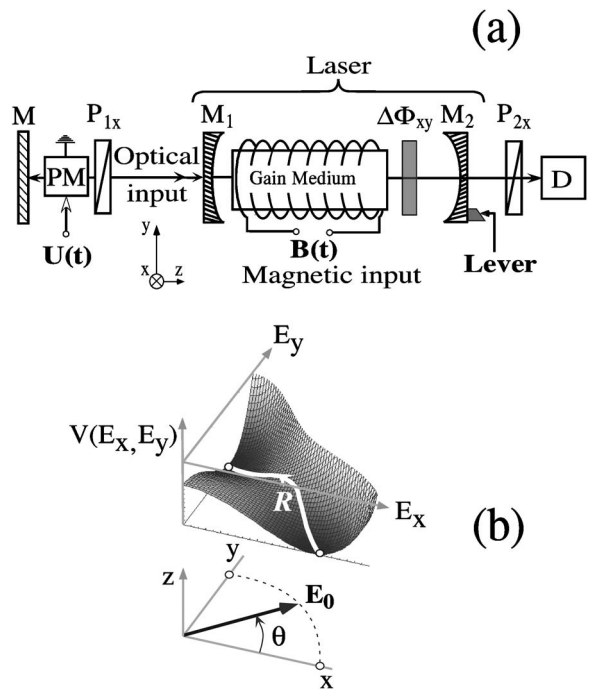

FIG. 1. The scheme of a vectorial bistable laser. (a) The laser cavity enclosed by two mirrors M_1 and M_2 contains a small linear phase anisotropy $\Delta\Phi_{xy}$ and a gain medium. The laser oscillates on a single longitudinal mode. Optical input is a reinjection cavity containing a voltage driven phase modulator PM, a mirror M, and a polarizer P_{1x}. The magnetic input is through a solenoid wrapped around the gain medium. The Zeeman splitting of the high gain 3.39 μm line of ^{20}Ne is 3.16 MHz/G leading to a Faraday effect [typically 1 deg/(m/G)] which can induce the rotation of the polarization. Lever control permits adjustment of the laser frequency using a piezoelectric transducer holding the mirror M_2 to change the laser cavity length. The laser axis is oriented along north-south direction, which adds about 0.2 G axial dc magnetic field also taken into account in the simulations. The output intensity along the x state is detected using an output polarizer P_{2x} and a detector D. (b) The three-dimensional (3D) potential associated with the vectorial laser. The light vector switches between the two stable states $\mathbf{E_x}$ and $\mathbf{E_y}$ by rotation in the transverse plane corresponding to the rotational path R on the potential surface.

linear phase anisotropy lifts the cavity transverse isotropy, yielding a two-dimensional system defined by two linearly polarized eigenstates $\mathbf{E}_x$ and $\mathbf{E}_y$ aligned along the x and y directions of the phase anisotropy. These eigenstates are calculated using the resonance condition $M\mathbf{E}=\Lambda\mathbf{E}$, where M is the 2×2 Jones matrix for one round-trip inside the cavity, and $\mathbf{E}$ is the electric-field vector with associated eigenvalues Λ [12,13]. Here, this transverse polarization distribution is invariant along the laser axis because the active medium does not alter the polarization. These two eigenstates oscillate at slightly different eigenfrequencies ν_x and ν_y with a frequency difference $\nu_x-\nu_y=(c/2L)\Delta\Phi_{xy}/\pi$, where c is the velocity of light in vacuum and L is the optical length of the cavity. In this paper we consider only the case of a quasi-isotropic laser, i.e., for a very small magnitude of $\Delta\Phi_{xy}$ such that $\nu_x-\nu_y$ becomes much less than the cavity bandwidth $\Delta\nu_c=(c/2L)[(1-R)/\pi\sqrt{R}]$, where R is the reflectivity of the two mirrors. By varying the laser cavity length the polarization can flip from one stable state to the other. For small phase anisotropy value, due to the strong nonlinear coupling between the two oscillators inside the gain medium, their frequencies get locked to a single frequency during the flip [14]. We then have a single oscillating light vector $\mathbf{E_0}$ which makes an angle θ from the x axis and can rotate in the transverse xy plane during the switches between the two stable states [see Fig. 1(b)], with a continuous frequency drift from one eigenfrequency to the other. The rotational dynamics of the polarization vector can be associated with a potential $V(E_x,E_y)$ such as the one depicted in Fig. 1(b) [12]. It has two minima corresponding to the two linearly polarized orthogonal stable states along the x and y directions, with the rotational switching schematized by the path R. The laser polarization can also be controlled by an optical input via a feedback cavity and by a magnetic input as shown in Fig. 1(a). During the polarization flipping, the laser intensity remains constant and the nonlinear dynamics of this optical rotor can be described by the following first-order differential equation for the angle of the light vector $\mathbf{E_0}$ with respect to the x direction [14,15]:

$$\frac{d\theta}{dt} = -V_0 \sin 4\theta + M(t)\sin 2\theta + \gamma B(t), \tag{1}$$

where γ is the Faraday rotation coefficient. The first term on the right-hand side of Eq. (1) leads to the rotational potential having minima at $\theta=0 \bmod \pi$ and $\theta=\pi/2 \bmod \pi$, separated by barriers of the heights $V_0/2$. The second term accounts for the optical input, and also for the cavity length tuning that we call the "lever" in Fig. 1(a). The last term is a Faraday term accounting for the magnetic field induced rotations of the vector, i.e., the magnetic input in Fig. 1(a). The temporal dependences of $M(t)$ and $B(t)$ will be fixed in the following by combinations of an input signal and single or multiple noises. Note that the delay time in the feedback cavity is assumed to be much smaller than the response time of the system. Thus the delayed feedback contribution can be neglected [16], in contrast to other schemes that exploit time-delayed feedback control [17].

How can we understand the symmetry properties of the perturbations $[M(t)$ and $B(t)]$ acting on the optical and magnetic functions in Eq. (1)? We try to answer this question by first considering the parities of these two forcing functions in the evolution equation. Here, in the laser the potential barriers are located at $\theta=\pi/4$ so we investigate the parities of the optical and magnetic functions with respect to an angle variable $\Theta=\theta-\pi/4$, and restrict our discussion in one quadrant of the potential $(-\pi/4\leqslant\Theta\leqslant\pi/4)$ as shown in Fig. 1(b). Note that due to the nonreciprocal nature of the Faraday effect in our system, if the axial magnetic field changes sign, it essentially inverts the direction of the optical rotation, i.e., the sign of Θ. This fact can be made to appear explicitly in the system equation by defining a function $\mathrm{sgn}(\Theta)$ which is $+1$ when $\Theta>0$, and -1 when $\Theta<0$. Equation (1) thus becomes

$$\frac{d\Theta}{dt} = V_0 \sin 4\Theta + M(t)\cos 2\Theta + \gamma B(t)\mathrm{sgn}(\Theta). \tag{2}$$

The optical forcing term (second term) in Eq. (2) is then *even* with respect to Θ but the magnetic forcing (third term) is *odd*. In the expression of the potential which can be obtained from Eq. (2) the parities of the forcing functions are reversed. This analysis of the rotor equation suggests that the even optical forcing should correspond to an asymmetric modulation of the potential and the odd magnetic forcing should lead to a symmetric modulation of the laser potential.

B. Hysteresis loop dynamics and stochastic resonances

1. Dynamics of the hysteresis loop

In order to isolate the role of the input function parity on the rotor dynamics, here we consider deterministic cases wherein only an adiabatic sinusoidal perturbation is acting on either the even or the odd function in Eq. (2) and focus on the dynamical evolution of the associated bistability cycle.

(a) Translation dynamics due to a forcing on the even function. When a sinusoidal perturbation of amplitude A_0 and angular frequency Ω_0 is injected through the optical input (even modulation), the temporal dependences of the coefficients in Eq. (1) become $M(t)=M_0\{A_0\cos(\Omega_0 t)+m_L\}$, and $B(t)=B_0$, where m_L is the so-called lever and B_0 denotes a residual constant axial magnetic field, which can be compensated. For all comparisons between the theoretical results and the following experimental results, we will use the normalized value of the modulation amplitude, i.e., $\tilde{A}_0=A_0/A_{th}$, where the switching threshold value is $A_{th}=2V_0/M_0$. Let us first simulate the unperturbed bistability cycle ($\tilde{A}_0=0$) of the model. This can be done by scanning the parameter m_L which corresponds experimentally to the cavity length variation and calculating the output intensity $I_x=E_0^2\cos^2\theta$ along the x eigenstate for instance. A numerically obtained symmetric hysteresis cycle is shown in Fig. 2(a).

Now in the presence of the sinusoidal modulation ($\tilde{A}_0=1.2$, $\Omega_0=2\pi\times 1$ kHz), the numerical integration of the model shows that such a perturbation produces a translation of the hysteresis loop with a period of 1 ms, as pictured in Figs. 2(b) and 2(c) for positive and negative maxima of the modulation. One can see that the width of the cycle remains constant. It is worth mentioning that such a translation of the cycle is an essential condition for the polarization switchings when the cavity length is kept fixed, as will be later the case for experimental observations. In the symmetric system of Fig. 2(a), i.e., when the bistability cycle is centered at zero, the switching thresholds correspond to a translation of the cycle by its half width. This translation dynamics of the bistability cycle corresponds to an asymmetric modulation of the bistable potential [15].

(b) Breathing dynamics due to a forcing on the odd function. By contrast, when the sinusoidal modulation is injected through the magnetic input function (odd modulation), the system now has the following coefficients: $M(t)=M_0 m_L$ and $B(t)=B_0+B_1A_0\cos(\Omega_0 t)$. Notably, this kind of perturbation produces a periodic breathing of the cycle with the period of 1 ms, as shown by numerical results in Figs. 2(d) and 2(e) for the maximum and minimum values of the input modulation. The width of the hysteresis loop oscillates with the input signal level while its center remains fixed. Here for a fixed laser cavity length corresponding to the symmetric potential we cannot observe any switching for such a modulation, contrary to the previous case.

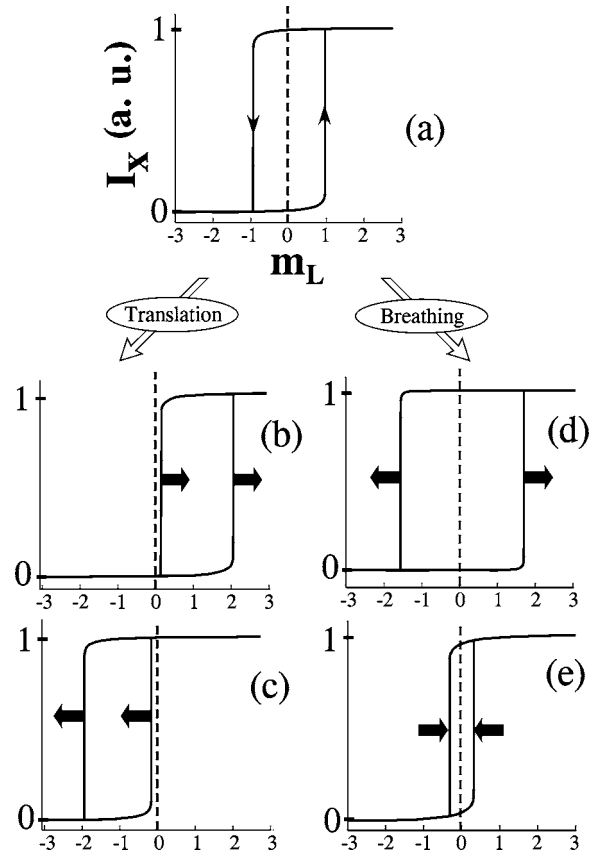

FIG. 2. Simulated translation and breathing dynamics of the hysteresis loop along the x state in the rotational regime observed by scanning the lever m_L in Eq. (1). (a) Unperturbed rotational bistability cycle obtained from Eq. (1) with the dimensionless parameters, $V_0=10^{-3}$, $M_0=10^{-3}$, $\gamma B_1=0.5\times 10^{-3}$, and integration time-step $\Delta t=10^{-8}$ s. (b)–(c) Translation dynamics of the cycle due to an input signal of normalized amplitude $\tilde{A}_0=1.2$ at the optical input function in Eq. (1) as shown for its positive (b) and negative (c) peak values, respectively. (d)–(e) Breathing dynamics of the cycle due to an input signal ($\tilde{A}_0=0.7$) at the magnetic input function for its positive (d) and negative (e) maxima.

These deterministic dynamics can also be helpful to picture the symmetry properties of random perturbations on the system. We thus apply two noises of different natures: the noise on the optical function (even noise) in order to produce the random translation of the cycle and the noise on the magnetic function (odd noise) in order to generate the random breathing dynamics. Thus it is possible with this system to investigate on the one hand the role of symmetry properties of different modulations and noises on the stochastic resonance phenomenon, and on the other hand the possible effects originating from the interplay between multiple noises of different kinds.

2. The role of the input function parity on stochastic resonance

In the following we shall investigate two different cases when a weak coherent modulation is injected into either the

TABLE I. Modulation $A_0\cos(\Omega_0 t)$ on the even function with one noise.

Optical noise	Magnetic noise
$M(t)=M_0[A_0\cos(\Omega_0 t)+\xi(t)]$	$M(t)=M_0[A_0\cos(\Omega_0 t)]$
$B(t)=B_0$	$B(t)=B_0+B_1\eta(t)$

even or the odd input function. In each case the noise is applied first on the even input and then on the odd input.

(a) Modulation on the even function. For a subthreshold even optical modulation we can use either the optical noise $\xi(t)$ or the magnetic noise $\eta(t)$ to try to induce SR. For these possible combinations of noises with signal in the symmetric system ($m_L=0$), the stochastic coefficients $M(t)$ and $B(t)$ in Eq. (1) are summarized in Table I.

These noises are zero mean white Gaussian noises: $\langle\xi(t)\rangle=0$, $\langle\xi(t)\xi(t')\rangle=2D\delta(t-t')$, and $\langle\eta(t)\rangle=0$, $\langle\eta(t)\eta(t')\rangle=2Q\delta(t-t')$, where D and Q denote their respective intensities. The probability density functions of the noises amplitudes have a Gaussian distribution. Furthermore, following the Wiener-Khinchin theorem [18], the power spectral density being the Fourier transform of the autocorrelation function, the spectra of these noises are flat. The stochastic differential equation Eq. (1) with the coefficients given by left-hand side column of Table I are numerically integrated using the first-order algorithm by applying the Stratonovitch interpretation to the noise terms as described in the Appendix. The SNR at the modulation frequency of 1.0 kHz is calculated for different optical noise levels from the power spectra obtained by averaging over 50 different temporal sequences of the simulated optical gates. The results are shown in Fig. 3(a) for three values of the subthreshold signal amplitude $\tilde{A}_0=0.9$, 0.45, and 0.2. The SNR exhibits the typical bell-shaped curve of stochastic resonance [2]. These results indicate that the weak even input signal can be detected by tuning the optical noise at its optimal level.

Now we consider the magnetic noise $\eta(t)$ instead of the optical noise to induce SR, i.e., we use the coefficients given by the right-hand side column of Table I in Eq. (1). As described in Fig. 3(b), the magnetic noise can also assist the weak signal and leads to the bell-shaped curves of SR, although this odd magnetic noise provokes a different random dynamics in the system. Thus we can say that if the coherent signal is acting on the even parity input, the SR mechanism can be induced by noises on either the even or odd parity function.

(b) Modulation on the odd function. Let us now consider that the modulation is acting on the odd input function, i.e., at the magnetic input. This modulation does not break the symmetry of the potential, as has been shown by the breathing dynamics of the bistability in Figs. 2(d) and 2(e). In this case, the time dependent terms in Eq. (1) including the noise at either the optical or magnetic input are given by Table II.

TABLE II. Modulation on the odd function with one noise.

Optical noise	Magnetic noise
$M(t)=M_0[\xi(t)]$	$M(t)=0$
$B(t)=B_0+B_1A_0\cos(\Omega_0 t)$	$B(t)=B_0+B_1[A_0\cos(\Omega_0 t)+\eta(t)]$

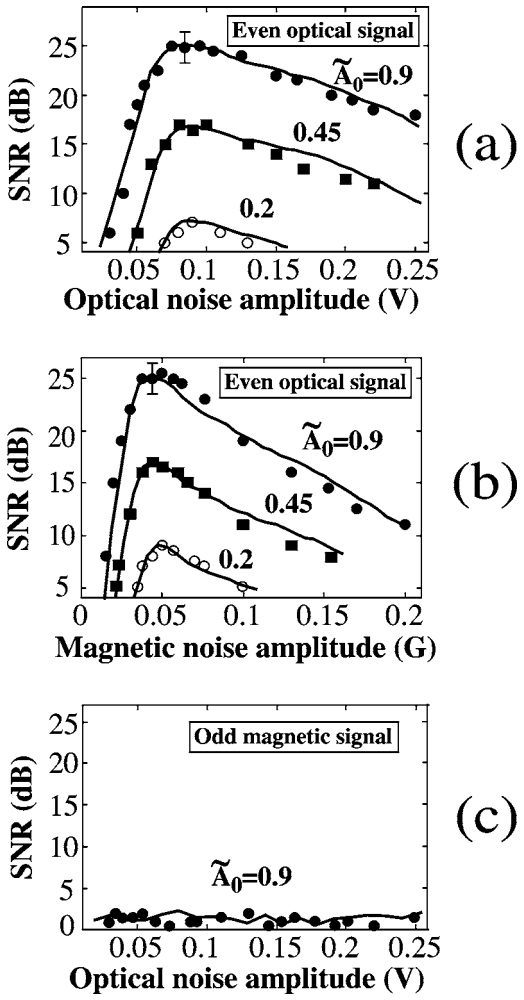

FIG. 3. The role of the signal parity on the existence of the stochastic resonance. (a) The presence of stochastic resonance due to the even parity signal with the optical noise only ($Q=0$). (b) Same as in (a) but with the magnetic noise only ($D=0$). (c) The absence of SR for an odd parity magnetic signal. Solid lines are numerical simulations (same values of the parameters as in Fig. 2), and filled circles ($\tilde{A}_0=0.9$), squares ($\tilde{A}_0=0.45$), and open circles ($\tilde{A}_0=0.2$) are experimental data. Note that the signal amplitudes are subthreshold and are normalized to the switching threshold for both experiment and simulation. The simulation fits to the experiment are obtained using the scale factors 75 V^{-1} for the optical noise and 42 mG^{-1} for the magnetic noise. The experimental data have been obtained averaging at least five independent spans of the power spectra. For the sake of clarity, the errors bars are represented on only one point. Note that the corrugation of the simulation curves have no physical meaning.

Here again we first try to use the optical noise to detect this symmetry preserving weak input signal. As expected from the cycle dynamics, simulation of the Eq. (1) with the coefficients of the left-side column of Table II shows no signature of stochastic resonance as the optical noise amplitude is varied. The bell-shaped SR curve falls flat, as shown in Fig. 3(c). This suggests that the stochastic resonance effect

cannot enhance such an input signal. Moreover, by using the magnetic noise instead of the optical noise corresponding to the column of the right-side of Table II we obtain the identical result, i.e., a flat SNR response with respect to the noise amplitude.

These simulation results show that the signal can be detected if it is applied to the even function in the laser system whatever the noise parity. These results will be tested in the experiment in Sec. III. In the following we consider another possibility provided by the multiple inputs of the vectorial laser, i.e., the nonlinear effects induced due to the interplay between two noises of the opposite parities. In Sec. II C and II D we analyze the system dynamics theoretically in the average residence times of the vector in its stable states and in the output signal-to-noise ratio expressions.

C. Interplay between mutually correlated noises

We consider the vectorial laser subjected simultaneously to two noises with strong mutual correlation acting on the two opposite parity functions in the Eq. (1). In this case, by considering the modulation applied on the optical input function the coefficients for the system are given as:

$$M(t) = M_0[A_0\cos(\Omega_0 t) + \xi(t)], \tag{3a}$$

$$B(t) = B_0 + B_1\eta(t). \tag{3b}$$

In addition, we include the following noise correlation in the model:

$$\langle \xi(t)\eta(t')\rangle = \langle \eta(t)\xi(t')\rangle = 2\lambda\sqrt{DQ}\,\delta(t-t'), \tag{4}$$

where λ denotes the strength of the correlation between these two noises. Here, we restrict our analysis to a particular case where both noises are fully correlated or anti-correlated, i.e., λ can take only two possible values of $+1$ or -1, respectively. Before numerically simulating this multinoise model, in the following we first derive analytical expressions for the residence-times and for the output SNR.

1. Derivation of the residence times and of the SNR

Our approach is to use the general two-state theory which is based on the transition rates as has been applied for asymmetric systems [19,20]. Briefly recalling the method, a bistable system having a potential as sketched in Fig. 4(a) is characterized by the occupation probabilities $n_x(t)$ and $n_y(t)$ of the two stable states x and y, respectively $[n_x(t)+n_y(t)=1]$. The equations governing the evolution of the occupation probabilities are given by

$$\frac{dn_x}{dt} = -\frac{dn_y}{dt} = W_y(t)n_y(t) - W_x(t)n_x(t) = W_y(t) - [W_x(t) + W_y(t)]n_x(t), \tag{5}$$

where $W_x(t)$ and $W_y(t)$ are the transition rates out of the two states x and y, respectively. For the multinoise rotor model of Eq. (1) with Eqs. (3) and (4), we now calculate the expressions for the transition rates $W_{x,y}(t)$. For this purpose, using the standard method [18,21] we calculate the mean residence

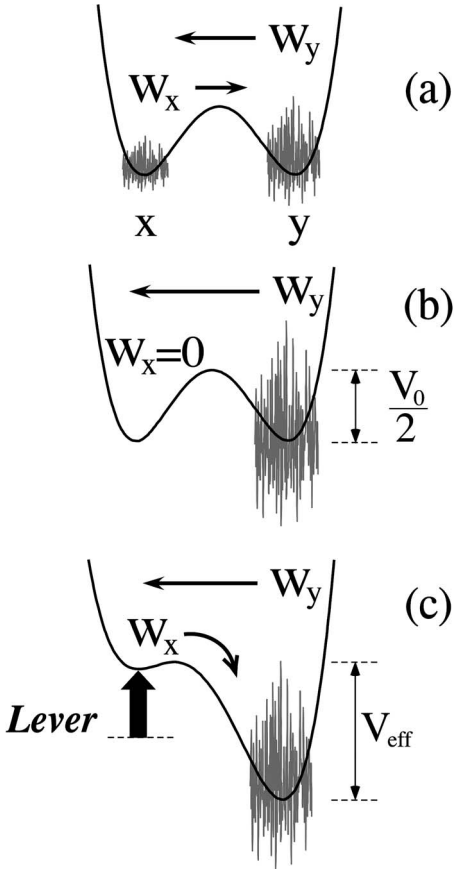

FIG. 4. An intuitive picture of the two-noise interplay in a two-well potential. (a) The correlation between noises makes the two transition rates different. (b) Critical regime: one well becomes noise-free at the expense of enhanced noise in the other well. The system remains trapped in the noise-free well ($W_x=0$). (c) Lever-assisted skewing of the potential in the critical regime restores the periodic switching cycle. The signal commands the escape out of the noise-free well while the reverse flips are due to the noise-induced events.

times T_x and T_y of the light vector in the two stable states at $\theta=0$ (x state) and $\theta=\pi/2$ (y state), respectively. When we consider the system to be symmetric ($m_L=0$) without any input signal ($A_0=0$), and take the coefficients $M_0=1$, $\gamma B_1=1$ in the dimensionless form of Eq. (1), we find the following expressions:

$$T_x = T\exp[2V_0 a_x(D,Q) - b_x(D,Q)], \tag{6a}$$

$$T_y = T\exp[2V_0 a_y(D,Q) - b_y(D,Q)], \tag{6b}$$

where T is a constant and $a_x(D,Q)$, $a_y(D,Q)$ and $b_x(D,Q)$, $b_y(D,Q)$ are given by

$$a_x(D,Q) = \frac{1}{D}\left(\log\left[\frac{|\sqrt{Q}+\lambda\sqrt{D}|}{\sqrt{Q}}\right] - \frac{\lambda\sqrt{D}}{|\sqrt{Q}+\lambda\sqrt{D}|}\right), \tag{7a}$$

$$a_y(D,Q) = \frac{1}{D}\left(\log\left[\frac{|\sqrt{Q}-\lambda\sqrt{D}|}{\sqrt{Q}}\right] + \frac{\lambda\sqrt{D}}{|\sqrt{Q}-\lambda\sqrt{D}|}\right), \tag{7b}$$

$$b_x(D,Q) = 2\log[|\sqrt{Q}+\lambda\sqrt{D}|], \tag{7c}$$

$$b_y(D,Q) = 2\log[|\sqrt{Q}-\lambda\sqrt{D}|]. \tag{7d}$$

In the presence of the input signal $A(t)=A_0\cos(\Omega_0 t)$, the two barrier heights of the potential are modulated asymmetrically. This dynamic asymmetry can be taken into account by assuming the asymmetric modulation of the barrier height parameter V_0 in the expressions of the two residence times. The transition rates $W_x(t)$ and $W_y(t)$ can be expressed as the inverses of these mean residence times resulting in the following expressions:

$$W_x(t) = T^{-1}\exp\{-2[V_0 + A_0\cos(\Omega_0 t)]a_x(D,Q) + b_x(D,Q)\}, \tag{8a}$$

$$W_y(t) = T^{-1}\exp\{-2[V_0 - A_0\cos(\Omega_0 t)]a_y(D,Q) + b_y(D,Q)\}. \tag{8b}$$

These rates can finally be expanded up to the first order in signal amplitude, leading to

$$W_x(t) = W_{0x} - \alpha_x A_0\cos(\Omega_0 t), \tag{9a}$$

$$W_y(t) = W_{0y} + \alpha_y A_0\cos(\Omega_0 t), \tag{9b}$$

where W_{0x}, W_{0y} are the inverse of the residence times without the modulation given by Eqs. (6a) and (6b), respectively, and $\alpha_x = 2a_x(D,Q)/T_x$, $\alpha_y = 2a_y(D,Q)/T_y$. Following Ref. [19], we perform a formal integration of Eq. (5) using Eqs. (9) that permits to calculate the SNR at the signal frequency. It is found to be independent of the signal frequency and, within the small signal amplitude assumption, it can be written as

$$\mathrm{SNR} = \pi A_0^2 \frac{[a_x(D,Q)+a_y(D,Q)]^2}{T_x + T_y}. \tag{10}$$

2. Discussion

One can notice that the mean residence times of the light vector in the x and y states subjected to two noises, but without the modulation, as given by Eqs. (6) and (7) are not identical (coefficients $a_x \neq a_y$ and $b_x \neq b_y$), even though the laser is symmetric with the identical barrier heights for the two stable states. Here the symmetry breaking between the two residence times is due to the mutual correlation between these two noises. In particular, if $\sqrt{Q}=\sqrt{D}$, T_x diverges to infinity when the noises are anticorrelated ($\lambda=-1$). This is referred to as the critical regime of the correlated noise interplay. Similarly, if these two noises are correlated ($\lambda=+1$), it is T_y which diverges in the critical regime. Consequently, in the critical regime of the correlated or anticorrelated noises, the SNR at the signal frequency which is given by Eq. (10) collapses to zero due to the diverging residence time in the denominator of the SNR expression.

Physically, the even and odd noises interfere constructively in one well and destructively in the other one. These noise interferences can be pictured as shown in the simple scheme in Fig. 4(a). Here the transition rates ($W_{x,y}$) out of the two wells are different although the bistable potential is symmetric. At the critical noise combination this transition rate asymmetry is maximum [see Fig. 4(b)], one state becomes completely *noise-free* ($W_x=0$) and, hence, the periodic polarization switching is no more possible.

Thus this theoretical analysis suggests that, although the system displays a specific property, namely the noise-free nature of one state, unfortunately the two-noise interplay seems detrimental in obtaining output switching cycle. This therefore raises the question of detecting the weak periodic modulation, i.e., to recover high SNR in this peculiar critical regime. In order to investigate this possibility, let us recall that up to now the laser system was taken to be symmetric. However, we have an independent symmetry control, i.e., the lever, which was previously used to observe the bistability cycle. In the following section, we investigate the effect of the lever induced asymmetry on the optical rotor in the critical regime of the multinoise interplay.

D. The dual stochastic response

Let us consider the intuitive image of the critical noise interplay in a two-well potential whose symmetry is broken through the lever, as shown in Fig. 4(c). Now the barrier corresponding to the noise-free state is almost vanished at the cost of enhanced barrier for the other state. It thus allows the weak modulation to command the escape out of the noise-free well. In contrast, the system can return back by surmounting the increased barrier due to the enhanced noise in the other well. We can then expect to restore the quasiperiodic switchings between the two states, but with a different kind of mechanism where the contributions of the signal and the noises are localized in different wells. To investigate the possible properties of the signal recovery in this regime, we first formulate the escape rate equations by taking into account both the noise-free nature of one state and the lever assistance in the system, and then derive an analytical expression for the output signal-to-noise ratio.

1. Derivation of the transition rates and of the SNR

In order to derive an approximate signal-to-noise ratio expression, in the presence of the lever we calculate new expressions of the escape rates $W_x(t)$ and $W_y(t)$ out of the noise-free well and of the noisy well, respectively. We assume that the lever is adjusted to skew the system such that the barrier corresponding to the noise-free state is reduced to zero. In this highly asymmetric situation, the approximate expressions for these two rates can be obtained as follows.

Considering first the noisy well, the escape is mainly noise driven as both noises interfere constructively here. For simplicity, we assume the escape rate out of the noisy well to be given by a Kramers-like formula, by taking into account

the lever modified effective barrier height V_{eff}, and the enhanced noise strength D_{eff},

$$W_{\mathrm{y}}(t) = W_{\mathrm{y}} = k \exp\left(-\frac{V_{\mathrm{eff}}}{D_{\mathrm{eff}}}\right), \tag{11}$$

where k is a constant depending upon the curvatures of the potential at its minima and maximum. The modified barrier height of the noisy state can be approximated as $V_{\mathrm{eff}}=V_0$, and since the noise amplitudes add coherently, the effective noise strength in this well in the critical regime, i.e., $\sqrt{D}=\sqrt{Q}$, can be taken as $D_{\mathrm{eff}}=(\sqrt{D}+\sqrt{Q})^2=4D$. Although the presence of a very weak modulation alters the effective barrier height periodically, we have neglected this effect because the signal strength is considered negligibly small compared to the barrier height in the noisy well.

Now considering the noise-free state, we have seen that the escape rate out of this state collapses to zero due to diverging residence time. But, due to the vanished barrier height, the very weak modulation can modify the transition rate significantly. During the negative half period of the modulation, a small barrier appears in the noise-free state and the polarization can remain trapped, leading to a zero transition rate. On the contrary, during its positive half period, the noise-free state barrier completely vanishes and this state then becomes unstable, leading to a very high transition rate. Thus the input signal switches the transition rate between zero and a very high value periodically depending on its sign. It can be approximated by using the following simple expression for the transition rate:

$$W_{\mathrm{x}}(t) \approx k'[1+\cos(\Omega_0 t)], \tag{12}$$

where k' is a constant. Thus the system dynamics in this lever-assisted critical regime is governed by the transition rates of Eqs. (11) and (12). By using the coefficients $W_{0\mathrm{y}}=W_{\mathrm{y}}$, $\alpha_{\mathrm{y}}=0$, $W_{0\mathrm{x}}=k'$, and $\alpha_{\mathrm{x}}=k'/A_0$ in the general expression of Ref. [20] and by considering the small noise limit as compared to the relaxation rate k ($k' \ll k$), we can calculate the SNR at the modulation frequency. This gives a remarkably simple formula

$$\mathrm{SNR} \cong \frac{\pi k}{4} \exp\left(-\frac{V_0}{4D}\right), \tag{13}$$

with $\sqrt{D}=\sqrt{Q}$.

2. Two original properties in the signal-to-noise ratio formula

The analysis performed above can provide us a valuable insight into the system behavior. It is useful to compare Eq. (13) with the standard SNR expression in the case of symmetric stochastic resonance: $\mathrm{SNR} \propto (A_0^2/D^2)\exp(-V_0/2D)$, known as the bell-shaped curve [2]. This highlights the following two original features of the system dynamics:

(a) Robustness. It is interesting to note that the $1/D^2$ dependence of SR which governs the postpeak decay of the bell-shaped curve is absent from Eq. (13). The noise dependence appears only in the exponential function. This means that the SNR first grows rapidly as the noise is increased and, for high noise levels it remains at its maximum value because the exponential dependence attains a limiting value of 1. This suggests that the system response now becomes nonresonant with respect to the noise amplitude.

(b) SNR plateau. Remarkably, Eq. (13) is also independent of the modulation amplitude A_0. It suggests that in this regime the system can display a plateau of high SNR with respect to the modulation amplitude and can allow the high fidelity detection of signal amplitudes far below the system threshold.

We emphasize that one of the fundamental requirements for such a regime [Eq. (13)] to occur is the noise-free nature of one stable state. Here in the vectorial laser it arises due to the critical interplay between two perfectly correlated optical and magnetic noises. Indeed, the perfect correlation is also realized when a single noise acts simultaneously on the two opposite parity input functions whose mutual interplay cancels in one state, i.e., due to the so-called *dual* action of a single noise in the laser system. Furthermore, in stark contrast with stochastic resonance, with the lever assistance the output response becomes nonresonant with respect to the noise level. We thus refer to the emerging regime of the optical rotor as its *dual stochastic response* (DSR). In the next section, we shall verify experimentally these theoretical predictions on the polarization rotor in the vectorial laser.

III. EXPERIMENTAL VERIFICATIONS

A. Experimental setup

The experimental scheme is depicted in Fig. 1(a). The laser cavity closed by mirrors M_1 and M_2 is 50 cm long. A slightly stressed silica plate is inserted inside the cavity in order to generate a weak linear phase anisotropy $\Delta\Phi_{\mathrm{xy}}$ fixed around 0.5°. Mirror M_1 has a radius of curvature 60 cm and transmits 30% of the incident light. The output mirror M_2 has the same transmission coefficient and a radius of curvature 120 cm, and is mounted on a piezoelectric transducer which controls the cavity length, i.e., the lever in Fig. 1(a). The laser cavity bandwidth is fixed by the cavity mirror reflectivities and the cavity length, and is $\Delta\nu_{\mathrm{c}} \approx 30$ MHz. The gain medium is a 20 cm long discharge tube with an inner diameter of 5 mm. It is filled with a 7:1 ^{3}He-^{20}Ne mixture at a total pressure of 1.1 Torr. The laser oscillates at wavelength 3.39 μm ($J=1 \rightarrow J=2$ transition) and emits a few μW power in a single longitudinal and fundamental transverse mode TEM_{00}. The weak atomic coupling of this line permits both σ components to oscillate simultaneously, and then to produce a stable linear polarization along either the x or y axes of $\Delta\Phi_{\mathrm{xy}}$.

To control the rotational polarization switchings, a feedback cavity of length 30 cm is employed which is depicted as the optical input in Fig. 1(a). It contains a plane mirror M of reflectivity 99%, a polarizer $P_{1\mathrm{x}}$, and a phase modulator (PM) using a $\mathrm{LiNbO_3}$ crystal. It is driven by a high voltage amplifier with a dc to 150 kHz bandwidth and upon which the signal and/or noise can be applied [see $U(t)$ in Fig. 1(a)]. Calibrated absorbing plates between $P_{1\mathrm{x}}$ and M_1 are used to attenuate the strength of optical reinjection down to about 1% of the emitted laser light. In addition, a solenoid is wrapped uniformly around the discharge tube and can generate an axial magnetic field of 0.011 G/mA of current

through the solenoid, shown as the magnetic input in Fig. 1(a). The so-called lever is here the laser cavity length controlled through the dc voltage applied to the piezoelectric holding M_2. It is used to tune the laser frequency by a few tens of megahertz across the Doppler broadened gain curve.

This laser is submitted to signal and noise via the optical and magnetic inputs. The noise has a Gaussian amplitude distribution and its spectrum is flat from dc to 100 kHz. The measured response bandwidth of the laser is around 40 kHz, thus validating our white noise assumption in the model. We have verified that the solenoid does not distort significantly the input noise spectrum (up to 100 kHz) which is used to generate a noisy axial magnetic field. The two correlated noises can be generated either using two noise Wandel and Goltermann RG-1 generators or using a single noise generator whose output is divided in two parts, one drives the PM to perform the optical noise while the other one generates the magnetic noise. When we use a common noise source the correlation strength between the optical and magnetic noises is measured and is found to reach $|\lambda| = 0.995$, which confirms a high degree of correlation in this case. This high correlation is reached because all the experimental apparatus is protected from acoustic and electrical perturbations. The output intensity along the x state is detected using an output polarizer P_{2x} and an InAs photodiode. It is then recorded digitally through a LeCroy 9450A oscilloscope connected to a LabVIEW data acquisition system and analyzed using a Hewlett-Packard 3588A spectrum analyzer.

B. One-noise stochastic resonances

1. Experimental verification of the bistability cycle dynamics

Let us first investigate the experimental hysteresis loop in the rotational regime of the laser. This is done by scanning the laser cavity length using a sweep voltage at the piezoelectric and monitoring the output intensity for instance along the x state, as shown in Fig. 5(a). Now in order to verify the possible hysteresis loop dynamics we apply only a sinusoidal modulation either to the optical or to the magnetic input of the laser, successively.

(a) Translation dynamics. When a sinusoidal modulation is applied to the optical input of the laser, we observe a periodic translation of the bistability cycle with a quasiconstant width, as shown for the positive and negative maxima of the modulation in Figs. 5(b) and 5(c), like the simulated cycles of Figs. 2(b) and 2(c). Consequently for a large amplitude, the optical signal can induce the coherent periodic polarization switches when the laser cavity length is kept fixed.

(b) Breathing dynamics. However, when the same signal is applied through the solenoid the laser exhibits a different dynamics. This kind of magnetic forcing produces a breathing of the cycle as shown in Figs. 5(d) and 5(e). The width of the cycle becomes proportional to the level of the input signal but its center remains fixed in the gain curve. We have verified that in this case no coherent polarization switch can be induced by this breathing dynamics.

These observations of the cycle dynamics provide an experimental support to the asymmetric and symmetric effects

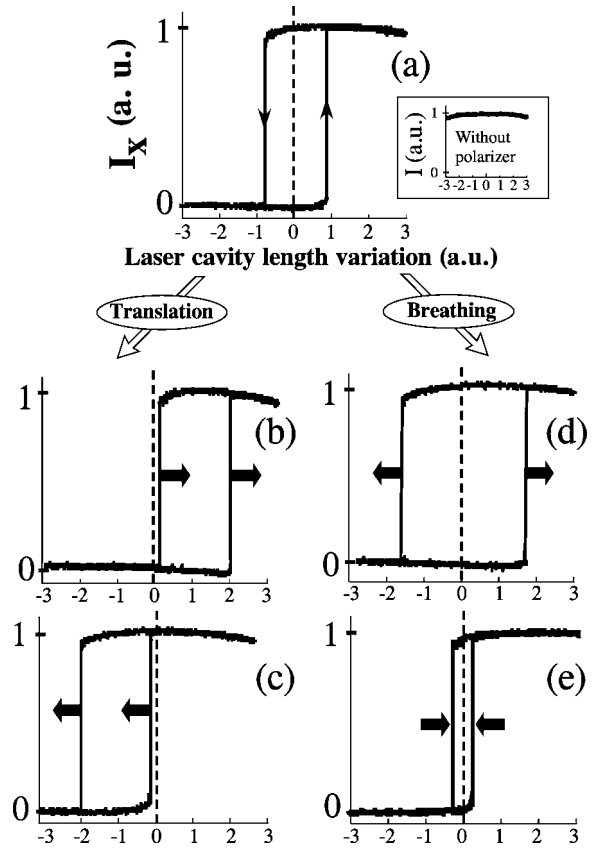

FIG. 5. Experimental dynamics of the hysteresis loop. (a) An unperturbed rotational bistability cycle observed by scanning the laser cavity length. The inset shows that the total intensity, obtained without the polarizer in front of the detector, remains constant during the flip. The center of the cycle (dashed line) corresponds to the maximum of the Doppler gain curve, (b)–(c) translation dynamics of the cycle due to an optical input signal for its positive and negative maxima, and (d)–(e) breathing dynamics of the cycle for a magnetic signal shown at its maximum and minimum values. Note that these dynamics reproduce well the simulated ones of Fig. 2.

on the potential due to the even optical and the odd magnetic forcings, respectively. It allows us to present in the following an experimental verification of the role of the parities of the input modulation and noise on the stochastic resonance mechanism.

2. Experimental evidence of the role of function parities

(a) The case of a subthreshold optical signal. Let us again consider the case when a signal is applied at the even optical input of the laser. For a subthreshold signal amplitude the cycle translation is not large enough, and the signal is not detectable via the coherent polarization switching. We can use either the optical noise $\xi(t)$ or the magnetic noise $\eta(t)$ at a time in the symmetric system to induce SR. The output SNR at the modulation frequency is measured first versus the optical noise amplitude, and second, versus the magnetic noise amplitude. Figures 3(a) and 3(b) show the corresponding experimental data for different modulation amplitudes, in agreement with the simulated curves (solid lines). Thus the subthreshold optical signal can be detected by using either the optical or the magnetic noise.

(b) The case of a subthreshold magnetic signal. When a subthreshold magnetic signal is applied to the laser, no switch is induced due to the breathing dynamics. In this case, we apply for instance the optical noise and measure the SNR of the laser output versus the noise amplitude. These measurements are shown by data points in Fig. 3(c), and prove the absence of a resonance-like effect. Indeed, no peak at the modulation frequency is observed in the output power spectrum. Moreover, by using the magnetic noise instead of the optical noise, we obtain an identical result, i.e., a flat response of the system.

These experimental and simulated results demonstrate that, independent of the noise parity, the signal must be even in this laser system to get the SR effect, in agreement with earlier theoretical predictions [22,23]. It clearly shows the crucial role of the input function parity in multi-input systems like the optical rotor studied here. In the next section, we explore the potentialities of the two correlated-noise interplay to overcome some limitations of the stochastic resonance.

C. Interplay between the correlated optical and magnetic noises

To investigate the noise interplay in the symmetric laser, in this section the cavity length is adjusted so that the maximum of the Doppler gain curve corresponds to the center of the bistability cycle, i.e., there is no lever.

1. Experimental residence times

The theoretical analysis of Sec. II shows that the mean residence time of the vector in one stable state diverges in the critical regime of the two-noise interplay. To verify this in the experiment, we first apply a subthreshold sinusoidal modulation at frequency 1.0 kHz and of normalized amplitude 0.9 through the optical input. As observed before, adding an optimal amount of optical noise restores the periodic polarization switchings due to SR. The mean residence times in the x and y states are measured from a recorded time series of the output intensity containing a few thousand switchings. For these measurements, the polarizer P_{2x} is kept fixed along the x axis. Indeed, on the optical gates, the "1" and "0" values correspond to the x and y eigenstates operations, respectively. The average residence times of the polarization vector in both states are equal and match the half period of the input signal (0.5 ms). Now the output of the same noise generator is used to produce the magnetic noise which is correlated with the optical noise. In the presence of the optical noise, increasing the magnetic noise amplitude induces an asymmetry in the residence times of the two stable states as demonstrated in Fig. 6. Notably, there exists a critical magnetic noise level $\sqrt{D_c}$ whose value is here 0.03 G where the residence time in one state becomes infinite, i.e., longer than the data-acquisition time of a few seconds. Beyond this so-called critical regime both the residence times decrease monotonously and for very high magnetic noise amplitudes they again become equal. A theoretical fit to the experimental data is obtained using Eqs. (6) and (7) with the perfect anticorrelation ($\lambda=-1$) between the two noises (see Fig. 6). This demonstrates a good agreement between the theoretical model and the experiment. Note that the noise-free well can be chosen via inverting the sign of the correlation between noises. Experimentally, the sign of the correlation can be chosen by inverting the polarity of the solenoid with respect to the optical input. Furthermore, we try to estimate the sensitivity of the system with respect to the correlation strength λ between noises. In this regard, we have also derived the residence-time expressions corresponding to any value of λ from the similar method of Eqs. (6). Using such expressions we show two additional fits in Fig. 6 for the values of λ slightly different from 1. The similar divergences in the mean residence times are also found to be present in the numerical simulations of the rotor model of Eqs. (1), (3), and (4).

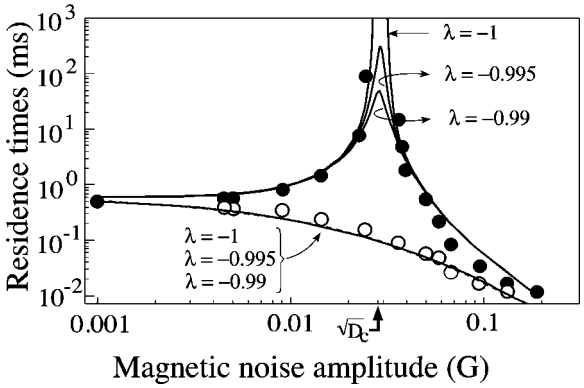

FIG. 6. Mean residence times vs magnetic noise in the presence of correlated optical noise. Filled and open circles denote experimental measurements in the x and y states, respectively. The optical noise is chosen at its optimum of one noise stochastic resonance. Lines are fits using Eqs. (6) and (7) with dimensionless parameters $\sqrt{D}=0.029$, $\lambda=-1$, $T=0.39\times10^{-3}$, and $V_0=0.02\times10^{-3}$. Note that here, since the modulation is not taken into account in Eqs. (6) and (7), and since the modulation amplitude is 0.9, we have to use an effective barrier more than one order of magnitude lower than the one used in Figs. 7 and 8. The axial magnetic field B_0 is compensated. Additional theoretical fits for slightly different value of λ are also shown.

2. Experimental SNR

For the optimized optical noise, a measurement of the SNR corresponding to the above observed two-noise-interplay is performed. This displays that the SR maximum of 25 dB collapses at the critical magnetic noise amplitude around 0.03 G, as demonstrated in Fig. 7(a). The same collapse is also observed when instead of varying the magnetic noise for a fixed optimum optical noise, we reverse the situation, i.e., the magnetic noise is first optimized to yield a 25 dB SNR and then the correlated optical noise is increased from zero [see Fig. 7(b)]. Theoretical fits for these two SNR measurements are derived from the approximate analytical expressions of Sec. II [Eq. (10)] and are shown by dashed lines in Figs. 7(a) and 7(b). It captures the essential features of the correlated noise interplay, notably the existence of the SR collapse at the critical noise combination.

Moreover, a numerical integration of the multinoise equations [Eqs. (1), (3), and (4)] is performed to describe the

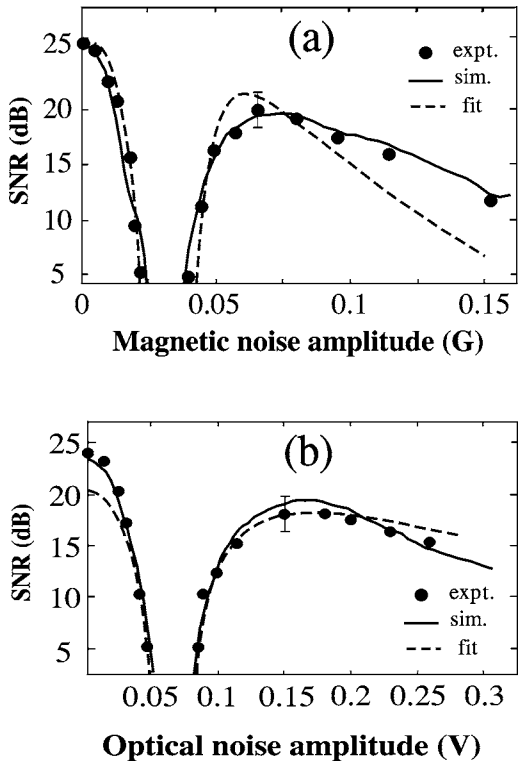

FIG. 7. The collapse of stochastic resonance due to the interplay between two correlated noises. Filled circles: experimental data, solid lines: numerical simulations, and dashed lines: theoretical fits. (a) SNR vs magnetic noise amplitude in the presence of optimal optical noise. The fits are derived from Eq. (10) with dimensionless parameter values $\sqrt{D}=0.033$, $V_0=0.85\times10^{-3}$, and $A_0^2/T=0.03$. (b) SNR vs optical noise level in the presence of optimal magnetic noise level, using Eq. (10) with parameters $\sqrt{Q}=0.065$, $V_0=1.5\times10^{-3}$, and $A_0^2/T=0.029$.

system dynamics in the presence of two correlated noises, with the procedure described in the Appendix. The correlated noises are generated using a single source of the Gaussian random number generator which applies to both the optical and magnetic input functions in Eq. (1). In parallel to the experimental measurements, the SNR is calculated using the phase averaged spectra by first fixing either the optical or the magnetic noise at its optimum level, and then by varying the second correlated noise. As shown by solid lines in Figs. 7(a) and 7(b), the two-noise collapse of SR in the critical regime fits well with the experimentally observed shape. It confirms the existence of the SNR collapse in the critical regime directly from the dynamical equations of the optical rotor. Note that the critical regime demonstrated here corresponds to a specific case when only one noise is at its optimum value of SR. However, such critical regime, i.e., the noise-free nature of one state can also be obtained for any other levels of noises provided that $\sqrt{Q}=\sqrt{D}$. In the next section, we focus on the signal recovery using the so-called dual stochastic response mechanism in the laser and verify experimentally its original features.

D. Experimental verification of the dual stochastic response

In order to verify the features of the theoretically predicted DSR, in this section a single noise perturbs both the even and the odd functions ensuring $\lambda=\pm1$ and we introduce the lever to break the symmetry of the system potential.

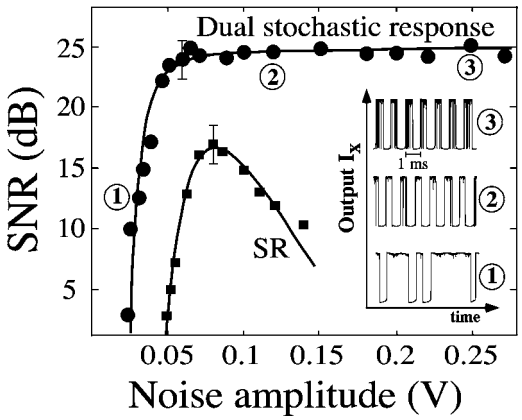

FIG. 8. Signal-to-noise ratio in the case of two-noise response (circles) and one-noise SR (squares). Inset: gates at points 1, 2, 3, of two-noise response. Note that the signal periodicity is preserved for higher noise levels. Solid lines are theoretical fits. For DSR the parameters in Eq. (13) are $V_0=1.6\times10^{-3}$, and $k=17$, fit for the SR is using the standard SNR formula (See Ref. [2]).

1. Robustness versus noise

First, to observe the high robustness of the DSR versus the noise amplitude, we note that in the corresponding SNR expression of Eq. (13) the optical noise intensity D and the magnetic noise intensity Q must be equal. Experimentally, we adjust the noise amplitudes once and if we then vary the noise amplitude applied to both functions, one stable state always remains noise-free. This can be directly monitored on the hysteresis loop dynamics. A combination of the even and the odd parity perturbations yields a superposition of the translation and the breathing dynamics of the cycle. The critical regime is obtained when one switching edge remains motionless.

To recover the switching cycle in the critical regime for a chosen input sinusoidal modulation of normalized amplitude 0.5 and at frequency 1.0 kHz at the optical input, we skew the system using the lever, i.e., the laser frequency, by applying a dc voltage to the piezoelectric transducer [see Fig. 1(a)]. The SNR of the laser output is measured versus the noise amplitude in Fig. 8. We can see in the experimentally recorded gates by the inset at point 1 in Fig. 8 that, when the noise level is small the switching cycle is not fully restored, because the noise in the so-called noisy state is not enough to induce a transition to the noise-free state every half period of the modulation. As the noise level in one state increases, the switching cycle is now fully restored as can be seen in the inset at point 2. For higher noise levels, the gates preserve the periodicity at the input modulation frequency (see inset for point 3). In this case the laser response displays rapid instabilities only within one half period corresponding to the unstable noise-free state, but the coherence at the modulation frequency is maintained. Thus the output SNR first increases rapidly with the noise amplitude and then stays at its maximum value of 25 dB. The experimental data are in good agreement with the theoretical fit of Eq. (13) shown by the

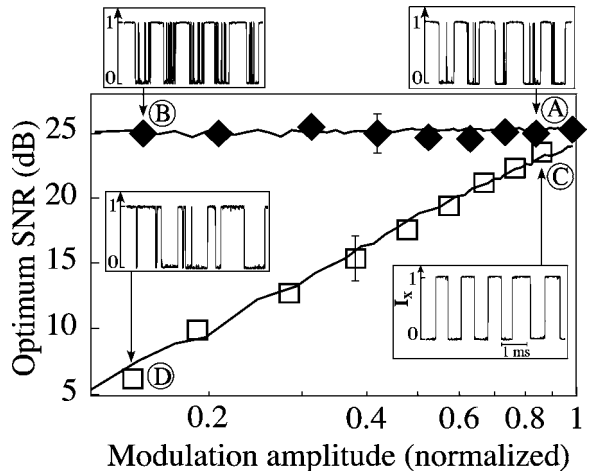

FIG. 9. Lever-assisted plateau in the critical regime. Two-noise response (diamonds) compared with the optimum SNR in the one-noise SR (square). Solid lines: numerical simulations. Parameters for the plateau: normalized lever $m_L=-0.99$, $\sqrt{Q}=0.03G$, $\sqrt{D}=0.07V$. Insets: experimentally recorded optical gates at points A–D.

solid line in Fig. 8. We have also compared the DSR of the laser with its one-noise stochastic resonance in the same figure (filled squares). This demonstrates that contrary to stochastic resonance, the laser dual stochastic response is nonresonant and robust against the variations of the noise strength.

2. SNR plateau versus the modulation amplitude

To experimentally observe the plateau we first adjust the laser in the critical regime corresponding for instance to the collapse of the SNR (Fig. 7). Now the independent lever is tuned to recover the highest possible SNR value of 25 dB for a chosen normalized signal amplitude value of 0.15. When the sinusoidal modulation amplitude is varied from 0.15 to close to the threshold, we observe that the SNR stays at the 25 dB level over around one order of magnitude variation in the signal amplitude, as shown in Fig. 9. The recorded gates corresponding to points A and B of the plateau are shown in the insets and clearly display the signature of the periodicity at the signal frequency. This observation is in agreement with the theoretical formula of Eq. (13), i.e., the SNR becomes independent of the modulation amplitude. In addition, the data also agree with the numerical simulation of the rotor model as shown by solid line in the Fig. 9. Here the maximum range of the plateau is limited by other residual parasitic uncorrelated noises in the noise-free state, although the simulations (avoiding the residual noises) show that it can in principle be extended to many orders of magnitudes of the signal amplitude. It is useful to compare the SNR plateau of the laser system with the optimum SNR obtained in the one-noise stochastic resonance. In stochastic resonance when the normalized modulation amplitude is lowered from 1 to 0.15 in the presence of the optimum noise, the maximum SNR degrades from 25 to 5 dB as shown by points C and D in Fig. 9. The insets at these points reflect a sharp decay in the induced synchronization at the signal frequency. Thus the DSR mechanism can provide a high output SNR for input signals far below the detection threshold.

Let us make here further remarks on the dual stochastic response. In Fig. 9 the DSR plateau is compared with the SR of the symmetric system. Note that in the so-called asymmetric SR which is useful for the dc signal detection [24–26], the system response to the fundamental modulation frequency degrades with the asymmetry. In addition, it is important to note that here the lever and the noise amplitudes are optimized only once for the lowest possible signal level, they are then left at these optimal values, and only the signal amplitude is varied to measure the plateau. We wish to emphasize that the phenomenon of the DSR is different from the stochastic resonance due to multiplicative or additive modulation and noise [27,28], as it is essentially nonresonant. The essential ingredient of the DSR is the noise-free nature of one state which is the result of the interplay between two input functions of opposite parities which can be both multiplicative as here in Eq. (2). Since the system now has one highly asymmetric barrier, the properties of the DSR are not only due to the vanished noise-free state barrier but also due to the enhanced noise in the other state which allows the system to surmount the higher barrier (see Fig. 4). Although the DSR is akin to what happens in excitable systems [2,29–31], here the switching from the noise-free state to the noisy-state is governed by the input signal, not by the internal dynamics of the system. Note also that we have not observed coherence resonance [32], because our system has always two stable states with fast intrawell relaxation times.

Is it possible to detect other types of input signals, for instance the symmetry preserving magnetic signals, using the DSR? Experimentally if we use the magnetic input signal, it induces the coherent switchings and we also find the similar plateau with respect to the signal amplitude. Thus unlike stochastic resonance, the DSR can also amplify the odd input signal. This can be readily understood by considering the two-well potential image of Fig. 4(c). As the magnetic signal modulates the central barrier height symmetrically (breathing dynamics), such modulation can also cause the periodic escapes out of the noise-free well by lowering the barrier in the asymmetric potential, and the return switch takes place as usual due to the noise. In addition, the DSR mechanism can also detect aperiodic inputs lying within the laser bandwidth up to 40 kHz. A typical system response for very weak aperiodic binary signal is measured experimentally as shown in Fig. 10. It is due to the fact that the switching out of the noise-free state can take place for any input modulation frequency. Indeed, the system now exhibits a wide band frequency response.

3. Residence-time distributions for DSR

Finally, what are the residence-time distributions (RTD) in this regime? To answer this question, we experimentally measure the RTD in both states of the polarization vector for three different normalized signal amplitude values ($\tilde{A}_0=0.9$, 0.45, and 0.15). In the SR case the results are shown in Figs. 11(a)–11(c). We observe that the residence times are identical for both states. Note that the peak at half period $T_0/2$ of the modulation vanishes for low subthreshold signals [see

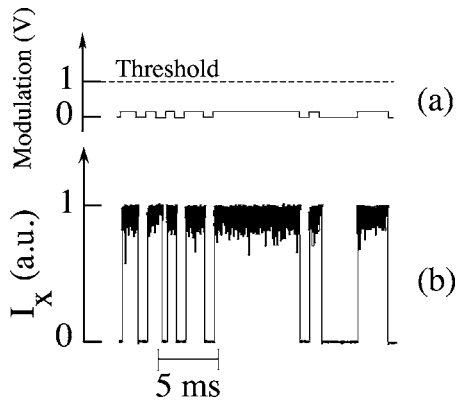

FIG. 10. Experimental DSR for aperiodic binary signals. (a) A subthreshold input signal and (b) the corresponding laser output along the x state.

Fig. 11(c)]. In the DSR case the RTD exhibits completely different features. Even far from threshold, we are left with a strong peak at $T_0/2$ as shown in Figs. 11(d)–11(f) for the noise-free state. Note that for the noisy state the RTD represented by the dotted curve keeps a Kramers-type dependence, as expected. Moreover, we have observed that by tuning the modulation frequency for a fixed noise the coherent peak in the noise-free state remains preserved at $T_0/2$, allowing the broadband frequency response [11].

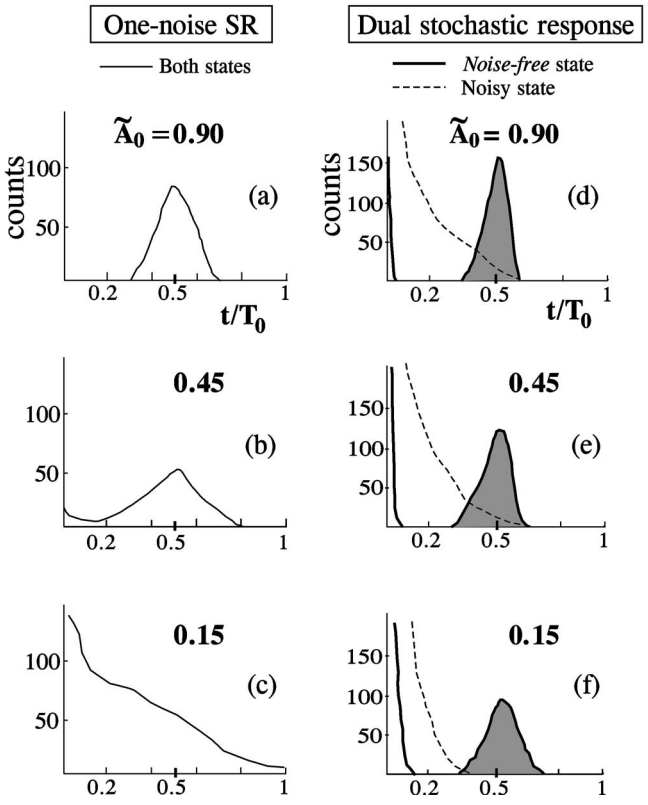

FIG. 11. Experimental residence-time distributions for the two states at three different signal amplitudes of 0.9, 0.45, and 0.15. (a)–(c) The case of one noise SR where the RTD is the same in both states. (d)–(f) For dual stochastic response, solid line: noise-free state and dashed line: noisy state. Note that in the case of DSR the peak at half the signal period is preserved even when the modulation amplitude decreases.

IV. SUMMARY AND CONCLUSION

The two-dimensional(2D) polarization rotation in the vectorial bistable laser allows us to investigate a theoretical and experimental study of a rich variety of nonlinear stochastic phenomena. Using the equation governing the rotational dynamics of the light vector, we demonstrated that the even and odd input forcing functions are able to induce the translation and breathing dynamics of the bistability cycle, respectively. We have exploited these multiple inputs of the optical rotor to study the effects due to the interplay between two mutually correlated noises of the opposite parities. The obtained theoretical expressions for the average residence times of the light vector in its stable states and the corresponding output signal-to-noise ratio predict the existence of a critical regime of the noise interplay corresponding to equal noise amplitudes. In this critical regime, one stable state becomes noise-free thus the residence time in this state diverges, leading to the collapse of the signal-to-noise ratio. The predicted features of the critical regime are confirmed experimentally by subjecting the laser to the mutually correlated optical and magnetic noises. However, in this critical regime alone the system does not respond to the input signal anymore.

We demonstrate that the system switching cycle can be recovered in the critical regime due to a new synchronization mechanism when the system symmetry is broken using an independent lever. In this case, a simple rate equation based analysis shows that the system response now becomes robust, i.e., *nonresonant* with respect to the input noise level. The laser DSR also exhibits a high sensitivity with respect to vanishing input modulation amplitude, leading to a SNR *plateau*. These results are in agreement with the experiment and numerical simulation of the rotor model. Moreover, the original signature of the DSR mechanism in the residence-time distributions is isolated. The noise-free state shows a robust peak at half the signal period. Due to the original synchronization mechanism of the DSR, the system also becomes sensitive to symmetry preserving modulations and to aperiodic input signals. These findings could widen the potentialities of noise-induced cooperative effects in nonlinear systems [33–38] provided that two functions with opposite parities govern the system dynamics.

ACKNOWLEDGMENTS

The authors thank Ludovic Frein and Claude Deroubaix for technical assistance. This work was supported by the Conseil Régional de Bretagne and the Délégation Générale de l'Armement (DGA).

APPENDIX

Here we describe the numerical algorithm used to integrate the Langevin equation for the vectorial laser. Our approach is basically the same as the one proposed in Ref. [39]. A formal integration of the corresponding stochastic differential equation between time interval t and $t+\Delta t$ yields the discretized version of the equation. We keep the terms only

up to the first order in time step of the integration. In the case of multinoise rotational Eq. (1), the angular evolution can be written in the following general form:

$$\frac{d\theta}{dt} = v(\theta,t) + g_1(\theta(t))\xi(t) + g_2(\theta(t))\eta(t), \qquad \text{(A1)}$$

where $v(\theta,t)$ is the deterministic function including the weak modulation and $g_1[\theta(t)]$ and $g_2[\theta(t)]$ are the two multiplicative stochastic functions with $\xi(t)$ and $\eta(t)$ being two Gaussian white random noises with the properties as defined in Sec. II. In our case these multiplicative functions have the forms: $g_1(\theta)=\sin(2\theta)$, and $g_2(\theta)=1$, using the Stratonovitch interpretation for the noise terms [39]. A formal integration of Eq. (A1) between times t and $t+\Delta t$ yields the discretized version of the equation suitable for the numerical analysis as

$$\begin{aligned}\theta(t+\Delta t) = \theta(t) + v(\theta,t)\Delta t + \{g_1(\theta(t))X_1(t) \\ + g_2(\theta(t))X_2(t)\} + \frac{1}{2}\{g_1(\theta(t))g_1'(\theta(t))X_1^2(t) \\ + g_2(\theta(t))g_2'(\theta(t))X_2^2(t)\} + \frac{1}{2}\{g_1(\theta(t))g_2'(\theta(t)) \\ + g_2(\theta(t))g_1'(\theta(t))\}X_1(t)X_2(t) + o(\Delta t^2). \qquad \text{(A2)}\end{aligned}$$

$X_1(t)=\sqrt{2D\Delta t}\gamma_1(t)$, $X_2(t)=\sqrt{2D\Delta t}\gamma_2(t)$, where $\gamma_1(t)$ and $\gamma_2(t)$ are two white Gaussian noises having unit variance and prime denotes the derivative with respect to θ. These numerical Gaussian noises are generated using a standard technique [40].

[1] K. Wiesenfeld and F. Moss, Nature (London) **373**, 33 (1995).
[2] L. Gammaitoni, P. Hänggi, P. Jung, and F. Marchesoni, Rev. Mod. Phys. **70**, 223 (1998).
[3] M. I. Dykman and P. V. E. McClintock, Sci. Prog. **82**, 113 (1999).
[4] J. F. Lindner, B. K. Meadows, W. L. Ditto, M. E. Inchiosa, and A. R. Bulsara, Phys. Rev. Lett. **75**, 3 (1995).
[5] J. J. Collins, C. C. Chow, and T. T. Imhoff, Nature (London) **376**, 236 (1995).
[6] R. Rozenfeld, A. Neiman, and L. Schimansky-Geier, Phys. Rev. E **62**, R3031 (2000).
[7] C. J. Tessone, H. S. Wio, and P. Hänggi, Phys. Rev. E **62**, 4623 (2000).
[8] A. Nikitin, N. G. Stocks, and A. R. Bulsara, Phys. Rev. E **68**, 016103 (2003).
[9] C. Zhou and C.-H. Lai, Phys. Rev. E **60**, 3928 (1999).
[10] K. P. Singh, G. Ropars, M. Brunel, and A. Le Floch, Phys. Rev. Lett. **90**, 073901 (2003).
[11] G. Ropars, K. P. Singh, M. Brunel, F. Doré, and A. Le Floch, Europhys. Lett. **68**, 755 (2004).
[12] A. Le Floch, G. Ropars, J. M. Lenormand, and R. Le Naour, Phys. Rev. Lett. **52**, 918 (1984).
[13] E. Hecht, *Optics* (Adisson Wesley, San Francisco, 2002).
[14] J. C. Cotteverte, F. Bretenaker, A. Le Floch, and P. Glorieux, Phys. Rev. A **49**, 2868 (1994).
[15] G. Ropars, A. Le Floch, and R. Le Naour, Phys. Rev. A **46**, 623 (1992).
[16] K. Panajotov, M. Arizaleta, M. Camarena, H. Thienpont, H. J. Unold, J. M. Ostermann, and R. Michalzik, Appl. Phys. Lett. **84**, 2763 (2004); O. Ushakov, S. Bauer, O. Brox, H.-J. Wünsche, and F. Henneberger, Phys. Rev. Lett. **92**, 043902 (2004).
[17] N. B. Janson, A. G. Balanov, and E. Schöll, Phys. Rev. Lett. **93**, 010601 (2004).
[18] C. Gardiner, *Handbook of Stochastic Methods* (Springer-Verlag, Berlin, 1983).
[19] B. McNamara and K. Wiesenfeld, Phys. Rev. A **39**, 4854 (1989).
[20] S. Bouzat and H. S. Wio, Phys. Rev. E **59**, 5142 (1999).
[21] Wu Da-jin, Cao Li, and Ke Sheng-zhi, Phys. Rev. E **50**, 2496 (1994).
[22] C. Presilla, F. Marchesoni, and L. Gammaitoni, Phys. Rev. A **40**, 2105 (1989).
[23] G. Debnath, T. Zhou, and F. Moss, Phys. Rev. A **39**, 4323 (1989).
[24] A. R. Bulsara, M. E. Inchiosa, and L. Gammaitoni, Phys. Rev. Lett. **77**, 2162 (1996).
[25] F. Marchesoni, F. Apostolico, and S. Santucci, Phys. Rev. E **59**, 3958 (1999).
[26] J.-H. Li, Phys. Rev. E **66**, 031104 (2002).
[27] L. Gammaitoni, F. Marchesoni, E. Menichella-Saetta, and S. Santucci, Phys. Rev. E **49**, 4878 (1994).
[28] M. I. Dykman, D. G. Luchinsky, P. V. E. McClintock, N. D. Stein, and N. G. Stocks, Phys. Rev. A **46**, R1713 (1992).
[29] A. Longtin and D. R. Chialvo, Phys. Rev. Lett. **81**, 4012 (1998).
[30] F. Marino, M. Giudici, S. Barland, and S. Balle, Phys. Rev. Lett. **88**, 040601 (2002).
[31] B. Lindner, J. García-Ojalvo, A. Neiman, and L. Schimansky-Geier, Phys. Rep. **392**, 321 (2004).
[32] A. S. Pikovsky and J. Kurths, Phys. Rev. Lett. **78**, 775 (1997); B. Lindner and L. Schimansky-Geier, Phys. Rev. E **61**, 6103 (2000); G. Giacomelli, M. Giudici, S. Balle, and J. R. Tredicce, Phys. Rev. Lett. **84**, 3298 (2000); O. V. Ushakov, H.-J. Wünsche, F. Henneberger, I. A. Khovanov, L. Schimansky-Geier, and M. Zaks, Phys. Rev. Lett. **95**, 123903 (2005).
[33] R. Rouse, Siyuan Han, and J. E. Lukens, Appl. Phys. Lett. **66**, 108 (1995).
[34] I. Zapata, R. Bartussek, F. Sols, and P. Hänggi, Phys. Rev. Lett. **77**, 2292 (1996).
[35] R. D. Astumian and P. Hänggi, Phys. Today **55**(11), 33 (2002).
[36] B. Q. Ai, X. J. Wang, G. T. Liu, and L. G. Liu, Phys. Rev. E **67**, 022903 (2003).
[37] K. Kitajo, D. Nozaki, L. M. Ward, and Y. Yamamoto, Phys. Rev. Lett. **90**, 218103 (2003).
[38] A. Zaikin, J. García-Ojalvo, R. Báscones, E. Ullner, and J. Kurths, Phys. Rev. Lett. **90**, 030601 (2003).
[39] J. M. Sancho, M. San Miguel, S. L. Katz, and J. D. Gunton, Phys. Rev. A **26**, 1589 (1982).
[40] W. H. Press, S. A. Teukolsky, W. T. Vetterling, and B. P. Flannery, *Numerical Recipes in Fortran 90* (Cambridge University Press, Cambridge, UK, 1997).